JOURNAL OF CATALYSIS 126, 246–260 (1990)

A High-Resolution Electron Microscopy Investigation of TiO_2(B)-Supported Vanadium Oxide Catalysts

L. REINE WALLENBERG,* MEHRI SANATI,† AND ARNE ANDERSSON†

*Department of Inorganic Chemistry 2 and †Department of Chemical Technology, Chemical Center, Lund Institute of Technology, P.O. Box 124, S-221 00 Lund, Sweden

Received February 13, 1990; revised June 5, 1990

TiO_2(B) crystals were found to be isomorphic with those of its precursor, $K_2Ti_4O_9$. The former crystals had a large number of facetted voids, 3–30 nm, formed as a result of the removal of potassium and water in preceding hydrolysis and calcination steps, respectively. TiO_2(B)-supported vanadium oxide catalysts with loadings in the range 0.25–10 theoretical layers were prepared by impregnation of the support with an oxalic acid solution of NH_4VO_3 followed by calcination in air. HREM micrographs of catalysts with a low vanadium loading, recorded using a low electron-dose imaging technique, showed that the surfaces, in the initial stage, were without any anomalous surface structure. This observation may be due to a similar structure of the support and the deposited vanadia phase. At high vanadium loadings, both amorphous and crystalline particles were seen, in agreement with the features revealed by the use of IR spectroscopy. For catalysts with low vanadium loadings, the IR difference spectra showed the presence of tetrahedrally coordinated V^{4+} and V^{5+} species. In a fully converged electron beam, reduction of the support and the vanadia phases occured, resulting in the formation of small crystallites. The catalysts were used for the oxidation of toluene to benzaldehyde. However, contrary to what has been observed for the ammoxidation producing benzonitrile, no enhanced catalytic properties, in comparison with those of crystalline V_2O_5, were obtained using TiO_2(B) as support.

INTRODUCTION

In recent years, TiO_2-supported vanadium oxide catalysts have been intensively studied because of their wide range of applicability in the chemical industry. They have mainly been used for the oxidation of alkylaromatic compounds, e.g., the oxidation of *o*-xylene to phthalic anhydride (*1–3*), and the oxidation of toluene to benzoic acid (*4*) and benzaldehyde (*5*). The same type of catalysts have also been found effective in the ammoxidation of 3-picoline and toluene to their corresponding nitriles (*6, 7*). For the production of phthalic anhydride (*2*) and benzoic acid (*4*), TiO_2 (anatase)-supported vanadium oxide catalysts were found to be superior when compared with both unsupported V_2O_5 and TiO_2 (rutile)-supported catalysts. This fact has been explained by the observation that vanadium oxide wets some of the crystal planes of anatase, but not those of rutile (*8*). In the former case this results in a preferential exposure of (010) faces of V_2O_5 (*9*). The existence of a crystallographic fit between the (010) plane of V_2O_5 and the (001) and (010) faces of anatase has been demonstrated (10). However, in a study of how preparation procedure and V/Ti-ratio influence the structure of the active phase, three different vanadium species were found in addition to crystalline V_2O_5 (*11*).

A new form of TiO_2, called TiO_2(B), was discovered some years ago (*12*). In a study of the oxidation of *o*-xylene to phthalic anhydride, TiO_2(B) was found to be as good a support as anatase for vanadium oxide (*13*). The investigators concluded that this was due to the existence of a crystallographic fit between the (010) plane of V_2O_5 (the notation is according to Bachmann *et al.* (*14*)) and the (001) face of TiO_2(B). Consequently, an epitaxial deposition of V_2O_5 exposing

0021-9517/90 $3.00

predominantly (010) faces can be expected. Also, in a study of the ammoxidation of toluene to benzonitrile, TiO_2(B)-supported vanadium oxide catalysts were found to be more active and selective compared with unsupported V_2O_5 (*15*). From the use of FTIR spectroscopy and chemical analysis, however, it was concluded that the growth of active phase on TiO_2(B) is more complex than simple epitaxial growth.

High-resolution transmission electron microscopy (HREM) is a useful technique for the characterization of both supported (*16,17*) and unsupported (*18*) vanadia catalysts. The present work, which is a continuation of our previous work (*15*), reports the characterization of TiO_2(B)-supported vanadia catalysts, using HREM and scanning electron microscopy (SEM). Also, catalytic data are reported on the use of prepared catalysts in the oxidation of toluene to produce benzaldehyde. Substantial amounts of benzaldehyde are used in the pharmaceutical industry. It is also used for the manufacture of odorants and flavoring chemicals (*19*).

EXPERIMENTAL

Preparation of catalysts. The support precursor, $K_2Ti_4O_9$, was prepared by calcining an appropriate mixture of anatase and KNO_3 at 950°C for 44 h. The product was ground and then hydrolyzed for 3 days at room temperature using a 0.45 N solution of HNO_3. To each mmole of $K_2Ti_4O_9$, 100 ml of the acid solution was added. After filtering and washing with water, the solid material was dried at 40°C for 24 h and further calcined at 500°C for 3 h. The resulting product, according to X-ray diffraction (*20*), was pure TiO_2(B).

TiO_2(B) was used as a support for vanadium oxide. The catalysts were prepared using the wet impregnation method (*15*). The desired amount of NH_4VO_3 was added to an oxalic acid solution having pH < 1. The support was added to this solution, and excess water was evaporated at 70°C while stirring. The resulting solid was dried at 40°C for 15 h and then calcined in a flow of air at 400°C for 3 h. After sieving, the fraction of particles with diameters in the range 0.150–0.425 mm was used in the experiment. Seven samples with different loadings of vanadium oxide were prepared. Their loadings, also included in the catalyst notation, and specific surface areas are given in Table 1. From the structure of V_2O_5 (*14*), an average value for a loading corresponding to a complete monolayer can be calculated as 1.2 mg V_2O_5 per square meter of the support surface area, if the (100), (010), and (001) planes are considered. Consequently, it follows from Table 1 that the loading was varied from $\frac{1}{4}$ of a theoretical layer up to 10 layers. The vanadium content of the catalysts was determined by atomic absorption spectrophotometry. For this purpose, the samples were completely dissolved in HF.

A monolayer sample, denoted VTM-1.2, was prepared by NH_3(aq)-treatment of a sample originally having a loading corresponding to five theoretical layers. Analysis showed that 80% of the vanadium was dissolved in the treatment. Eventually, the sample was calcined in air at 400°C for 3 h. As a reference, a crystalline and pure V_2O_5 sample was prepared by decomposing NH_4VO_3 (Merck p.A.) in air at 450°C. Its specific surface area was 5.7 m^2/g.

TABLE 1

Loading and Surface Area of Catalysts

Catalyst	Loading[a] (mg V_2O_5/m^2)	S_B[b] (m^2/g)	S_A[c] (m^2/g)
VT-0.3	0.30	11.0	9.7
VT-0.6	0.62	15.3	9.8
VT-0.9	0.93	18.3	13.1
VTM-1.2	1.20	13.7	10.9
VT-1.9	1.87	18.3	11.0
VT-4.2	4.24	13.7	12.7
VT-12.4	12.41	13.7	15.7

[a] Expressed per surface area of fresh support.
[b] Specific surface area/g support before impregnation.
[c] Specific surface area/g catalyst after impregnation.

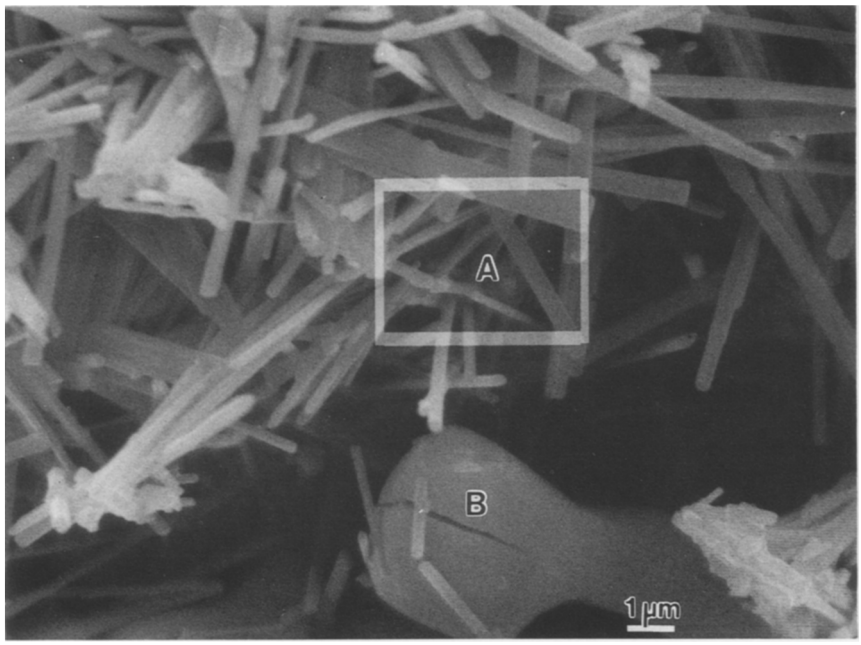

FIG. 1. Scanning electron micrograph of the support precursor. The rod-like particles in the boxed area (A) have a Ti/K ratio corresponding to $K_2Ti_4O_9$, whereas a minor phase with a higher Ti/K ratio consists of relatively large and smooth particles (B).

Characterization of catalysts. Catalysts with loadings corresponding to 1, 1.5, and 10 theoretical layers were selected for investigation by electron microscopy. Scanning electron microscopy was performed with a JEM 840A microscope with a Link AN 10000 Energy Dispersive X-ray Spectrometer (EDS) for elemental analysis. Quantification of EDS spectra was done with a ZAF 4/FLS program.

High-resolution micrographs were recorded with a JEM 4000EX transmission electron microscope in a top-entry configuration, giving a structural resolution limit of 0.16 nm at 400 kV accelerating voltage. A Gatan 622 image-intensified TV-camera was used for obtaining low electron-dose images. A JEM 2000FX Scanning Transmission Electron Microscope (STEM) with a 0.27-nm resolution limit at 200 kV was used for tilting experiments. For imaging, the samples were gently dispersed in methanol so as not to create new fracture surfaces, and a drop of the dispersion was placed on an amorphous holey carbon grid.

FTIR spectra were recorded using a Mattson Polaris spectrometer equipped with a Harrick Scientific Praying Mantis diffuse reflection attachment. Due to the fact that vanadium oxides are highly absorbing materials, it was necessary to dilute with KBr to give 5–15 wt% of sample. Spectra were recorded without further treatment in dry air free of CO_2. A resolution of 4 cm^{-1} was used, and 1000 spectra were collected for each sample. ICON analytical software from Mattson Instruments was used for spectral treatment.

Activity measurements. The catalytic performance of prepared catalysts was studied in the oxidation of toluene to benzaldehyde. Carbon oxides were formed as the main byproducts. A differential and isothermal plug flow reactor held at 370°C was used in the experiments. A total flow of 186 standard cm^3/min was passed over 0.1–0.5 g of cata-

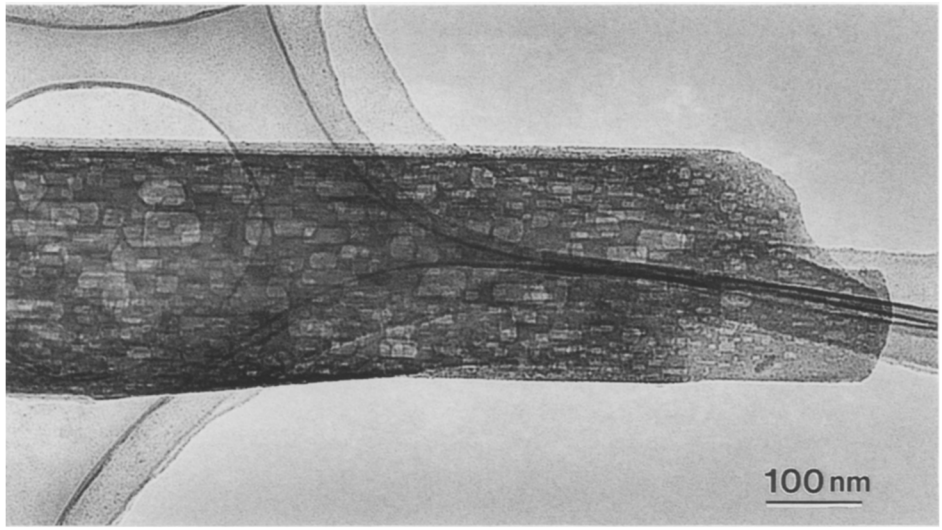

FIG. 2. Transmission electron micrograph of a rod-like TiO_2(B) crystal. The formation of facetted voids ("negative crystals") accounts for 32% reduction in volume with maintenance of particle size and morphology.

lyst, diluted with quartz of the same particle size. The partial pressures of toluene and oxygen were 0.77 kPa and 11.42 kPa, respectively. Nitrogen was used as an inert gas. Reaction products were analyzed on a Varian Vista 6000 gas chromatograph. Reactor and analysis arrangement were the same as described elsewhere (*21*).

RESULTS

Electron Microscopy

Support precursor. On investigation by SEM, Fig. 1, two different phases were easily distinguished by their different morphology. The major part of the precursor consisted of extremely rod-like particles with typical dimensions of 0.2 × 0.2 × 8 μm, while the less frequent type of particles were larger and appeared smoother. Analysis by EDS showed that the Ti/K ratio of the rod-like particles was 1.94, corresponding to $K_2Ti_4O_9$. The corresponding ratio for the smooth particles was 2.56, thus they possibly consisted of $K_3Ti_8O_{17}$.

HREM micrographs showed that the rod-like particles consisted of bundles of intergrown, very narrow single crystals, which made identification through the selected area electron diffraction (SAD) patterns very difficult. Occasionally, larger single crystal areas could be found. The cell dimensions determined from [001] zone axis SAD patterns were a = 18.7 Å and b = 3.88 Å, which are within 2.7% of the literature data given below. The shortest axis, 3.88 Å, was always oriented parallel to the long axis of the rod. $K_2Ti_4O_9$ has been reported as being monoclinic, of space group $c2/m$ with a = 18.25 Å, b = 3.791 Å, c = 12.01 Å, and β = 106.4° (*22*).

TiO_2(B) support. On hydrolysis ($K_2Ti_4O_9 \rightarrow H_3OTi_4O_8OH$) and calcination of the precursor to form TiO_2(B), a large part of the volume (~32%) is lost due to elimination of potassium and water. Surprisingly, SEM micrographs showed TiO_2(B) to be isomorphic with the rod-like particles of $K_2Ti_4O_9$, though some fractioning and surface roughening appeared. High-resolution images taken at defocus values higher than the optimum to enhance lower frequency features in the image, Fig. 2, revealed that the loss

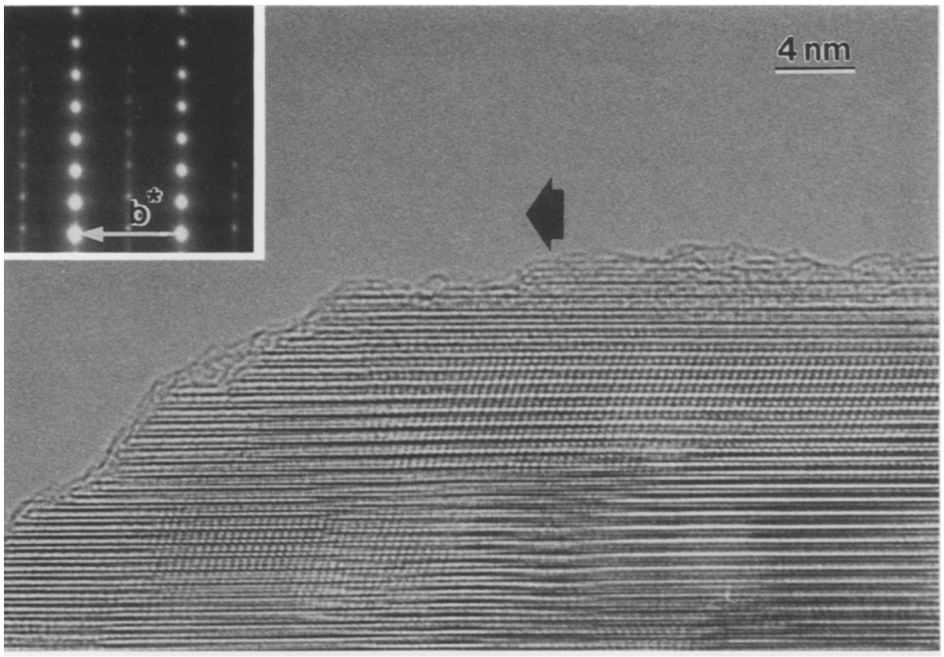

FIG. 3. High-resolution image of the surface of a TiO_2(B) rod. No anomalous surface structure is visible. In the thicker part, the structure image varies due to the voids in the bulk of the crystal. The black arrow indicates the long axis of the rod. Inserted is a section of the selected area diffraction pattern, recorded along the [100] zone axis, showing diffuse streaking perpendicular to b^*.

of volume is accomplished by the formation of a large number of 3–30 nm large facetted voids ("negative crystals"). Stereo images showed that the voids were formed throughout the bulk of the material.

Exposure to a fully focused beam (beam current density ~30 Å/cm^2) for 5 min did not have any effect on the size, nor on the distribution of the voids. Selected area diffraction patterns and HREM images revealed that the shortest axis, which is 3.735 Å in TiO_2(B) (*12*), is maintained along the long axis of the rod. Quantitative EDS measurements showed the residual potassium concentration to be less than 0.7 at.%.

For faithful imaging of clean surfaces of crystals with atomic resolution, great care must be exercised when exposing the sample to the electron beam. The growth rate of amorphous contamination, using a fully focused beam (beam current density ~30 Å/cm^2) and a vacuum better than 3×10^{-5} Pa, was found to be 50–150 Å/min. Previous work (*23, 24*) has also established beam-induced reductions of V_2O_5 and TiO_2(rutile) to $VO_{0.9}$ and TiO, respectively. To avoid beam-induced artifacts, astigmatism adjustment was performed on the amorphous carbon support at high beam intensity just before the beam was moved, now with a low current density, into nearby previously unexposed areas of the sample. The image-intensified TV-system made accurate focusing possible at a reduced intensity and at fairly low instrument magnification (3–500, 000×). The intensity was only increased seconds before exposure of the photographic plates. Using this low-dose technique, the average beam current density could be reduced by 1–2 orders of magnitude.

A surface profile image of the TiO_2(B) support recorded in the [100] main direction under low-dose conditions is shown in Fig.

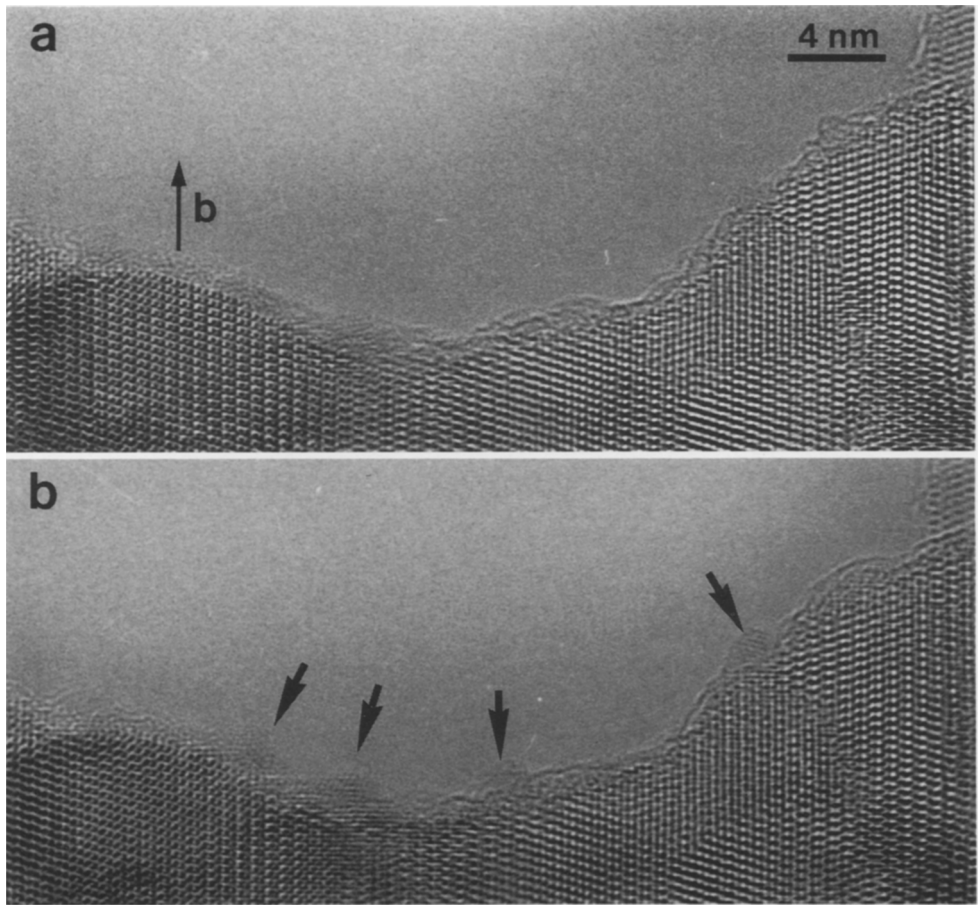

FIG. 4. HREM micrograph of the TiO_2(B) surface after exposure to a fully converged electron beam for (a) 0.3 min, and (b) 4 min. Formed particles are arrowed. Selected area convergent beam electron diffraction patterns suggests [001] to be the predominant viewing direction. The direction of the *b*-axis is indicated.

3. The lattice seems continuous all the way to the edge of the crystal without any anomalous surface structure. The mottling of the structure image is due to the rapid thickness variation caused by the voids in the crystal. Hence, single crystal areas of equal thickness are only of the order 75 × 100 Å, which makes image interpretation and alignment of zone axes difficult. The SAD patterns, of which one is inserted in Fig. 3, always showed streaking perpendicular to the b^*-axis, indicating some disorder perpendicular to the long axis of the rods. A weak diffuse intensity was always present along the forbidden $0kl$, $k = 2n + 1$ rows of reflections. This intensity is partly due to rotational disorder of the monoclinic cell around the *b*-axis, giving intensity from allowed $h = 2n + 1$ rows of spots in the $k = 2n + 1$ Laue zones.

Figure 4a shows that the surfaces of TiO_2(B) were initially clean and free from crystalline particles. After approximately 4 min of exposure to a fully converged beam, crystallites with 10- to 12-Å diameter appeared, as shown in Fig. 4b.

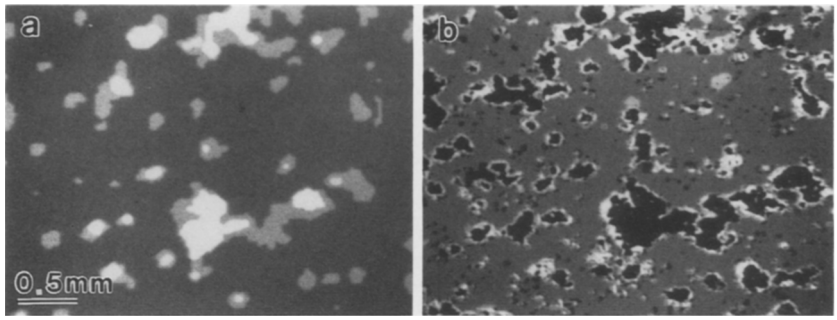

FIG. 5. (a) EDS-map of the VT-12.4 catalyst, showing the distribution of vanadium (light). (b) An overlay with the map for titanium (dark) confirms that the support is covered with vanadium.

VT-12.4 catalyst. Investigation of the sample by SEM showed that the impregnation and the calcination procedures had no influence on the morphology of the support. The amount of vanadium determined by quantitative EDS was 9.3 at.%, which is consistent with the amount supported. Elemental mapping of Ti and V (Fig. 5) showed that the vanadium was evenly distributed on the support, and no large precipitates of pure vanadium oxides could be detected.

High-resolution micrographs showed that the major part of the surface area was without any distinct surface structures or particles. However, beam-induced particle formation occurred which was distinctly much more rapid on vanadium-covered catalysts than on the pure support. Particles grew in size up to about 30–50 Å in diameter after 2–4 min in the electron beam, as shown in Fig. 6. Also, a few larger particles, approx. 500 Å in diameter, not formed by the beam, were found in amounts which did not account for the deposited amount. They were both crystalline and semiamorphous as shown in Figs. 7a and 7b, respectively. Similar structures were absent on the pure TiO_2(B) support.

VT-1.9 catalyst. Low-dose HREM images showed the major area of the surface to be clean and without particles; Fig. 8. On irradiation, particles appeared more prevalently in areas where the crystallinity of the support was poor. In Fig. 9, a typical particle is shown, exhibiting a crystal habitus and structural image typical for the rock salt structure (fcc cations). Optical diffractograms of the photographic plates, using the short axis of the TiO_2(B) support as an internal standard, indicated a spacing of 2.42 ± 0.08 Å between {111}-type fringes. This is consistent with VO_x, viewed along the [110] direction (25). This form of VO_x has a variable composition with $0.8 \leq x \leq 1.20$ and with a varying between $4.042 \leq a \leq 4.126$ Å.

Monolayer catalyst (VTM−1.2). No apparent difference between the HREM images of the VTM-1.2 and the VT-1.9 samples could be detected. The surfaces of the VTM-1.2 sample were initially clean, but as a result of the electron beam irradiation, 10-20 Å particles were produced as shown in Fig. 10.

Infrared Spectra of Vanadium–Oxygen Vibrations

Diffuse reflectance FTIR spectra of the VTM-1.2, VT-1.9, and VT-12.4 samples were recorded in the region of fundamental metal–oxygen vibrations. Difference spectra, obtained after subtraction of the TiO_2(B) spectrum and the V_2O_5 spectrum when present (VT-12.4), are shown in Fig. 11. The spectrum for the monolayer catalyst, VTM-1.2, shows an intense band at 820

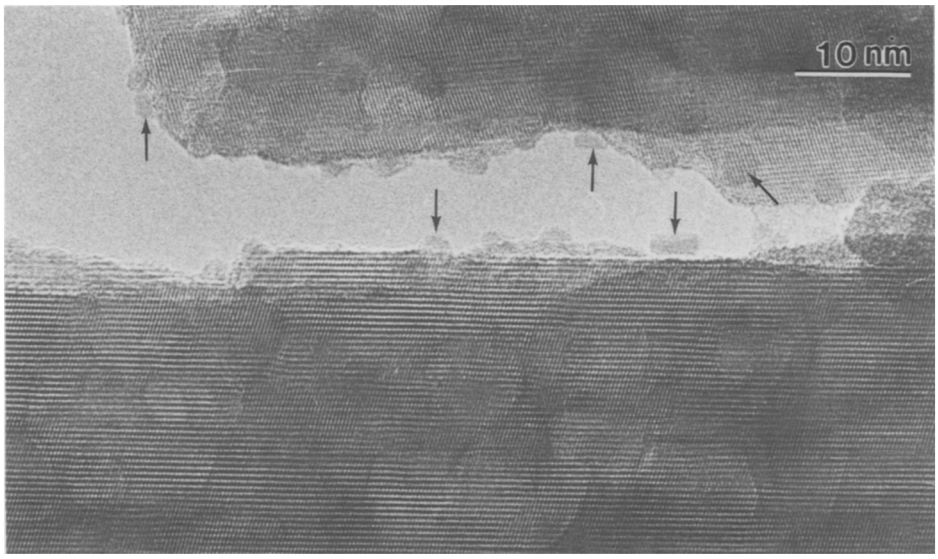

FIG. 6. HREM image of the VT-12.4 catalyst after 2 min of exposure to the electron beam. Reduced vanadium oxide particles, of which a few are marked by arrows, were rapidly formed at the surface of the support. The contours of the voids are weakly visible in the support.

cm^{-1} and a weaker band at 1000 cm^{-1}. Two bands, at 835 and 960 cm^{-1}, were resolved for the VT-1.9 sample, while the spectrum for VT-12.4 has a strong band at 970 cm^{-1} and a weak band at 764 cm^{-1}.

Performance of Catalysts in the Oxidation of Toluene

Figure 12 shows the rates of formation of benzaldehyde as a function of the vanadium content. For comparison, the rate obtained for the V_2O_5 reference sample is included. The rate of formation of aldehyde increases with increase in vanadium content. At high loadings, the values are close to that for pure V_2O_5. Over the VTM-1.2 catalyst only total oxidation took place and no formation of benzaldehyde was observed. In comparison with other samples, pure TiO_2(B) had a very low activity.

The variation of the selectivity for the formation of benzaldehyde is shown in Fig. 13 as a function of the vanadium loading. The selectivity increases with increase in vanadium content, mainly due to the decrease of carbon oxide formation. Crystalline V_2O_5 is slightly more selective than the VT-4.2 and VT-12.4 catalysts. In addition to aldehyde and carbon oxides, small amounts of maleic anhydride, benzoquinone, and benzoic acid were also formed. The total selectivity for the formation of the latter products in no case exceeded 10%, as determined from the carbon balance.

DISCUSSION

Structural Features

The specific surface area of the pure TiO_2(B) support was in the range 11–18 m^2/g (Table 1). In a previous investigation, using the same preparation method, a value of 19 m^2/g was obtained (*13*). These values are intermediate compared to those reported for the anatase and rutile modification. For anatase, an area above 50 m^2/g is not unusual (*11, 26, 27*). The specific surface area of rutile is usually less than 10 m^2/g (*28, 29*) even though a considerably higher value, 49 m^2/g for a coprecipitated 5 wt% V_2O_5/TiO_2(rutile) catalyst, has recently been reported (*30*). In this regard, it may be of interest to explore to what extent the

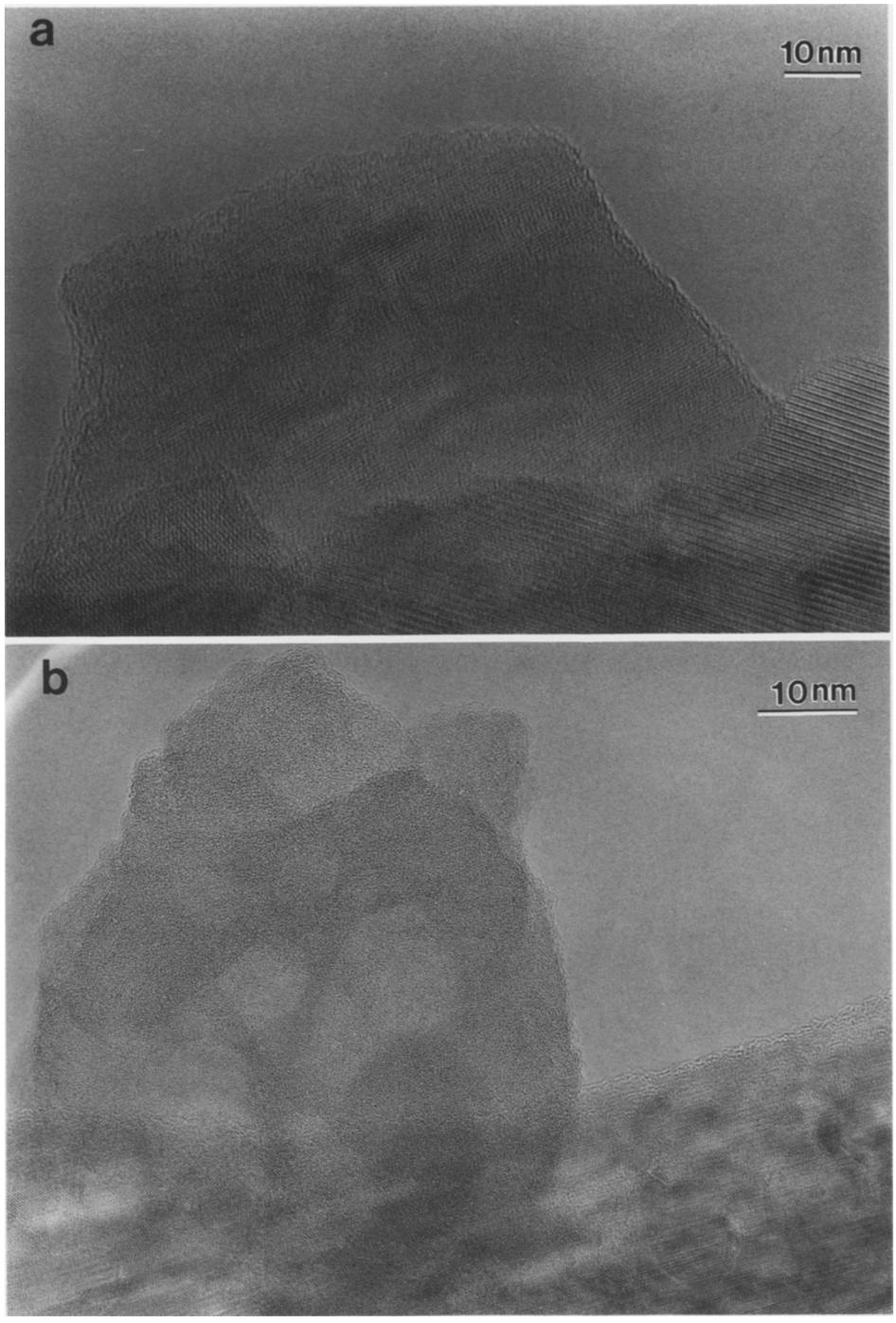

FIG. 7. (a) A crystalline particle, approximately 700 Å in diameter. (b) A semiamorphous particle. No similar types of particle were found on the pure TiO_2(B) support or at low loadings of vanadium oxide.

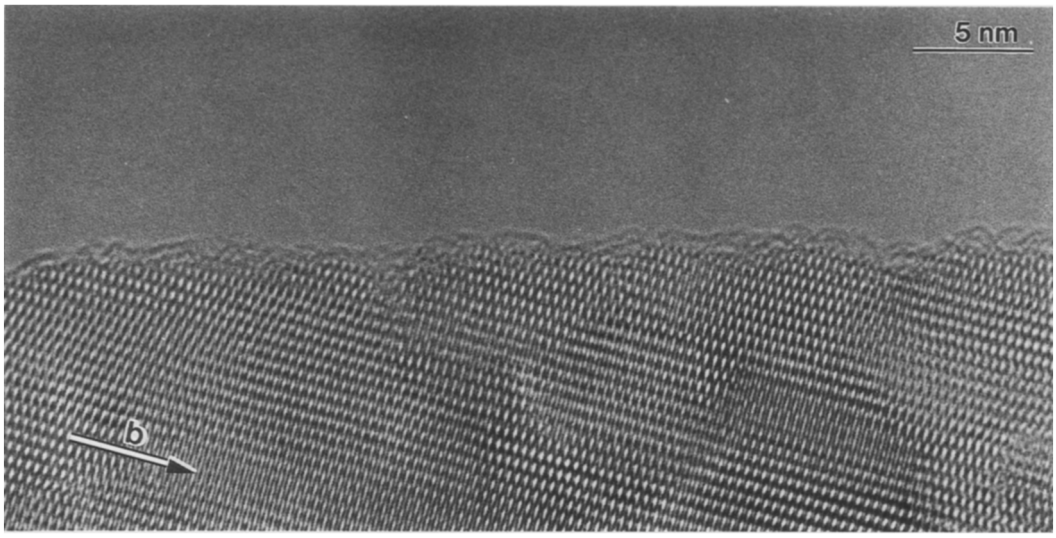

FIG. 8. A typical surface of the VT-1.9 catalyst recorded with the low-dose technique. No anomalous surface structure or particles are initially seen. The direction of the *b*-axis is indicated by the arrow.

voids (Fig. 2), formed in TiO_2(B) as a result of removal of potassium and water in the hydrolysis and calcination procedures, are open and thus accessible to the reactants. If they are closed, their opening would undoubtedly be a possible way to increase the specific surface area. From an average crystal size of 0.2 × 0.2 × 0.8 μm, it follows that the external crystal area is 5 m^2/g. If all the voids were interconnected and accessible to the reactants, a value of 53 m^2/g for the specific surface area would be obtained assuming a mean void diameter of 100 Å. A comparison with the values in Table 1 shows that possibly some voids are open. In an attempt to increase the contribution from voids to the total surface area, modifications of the preparation method have been tried (*31*). It was observed that it is possible to increase the area up to ~30 m^2/g by increase of the potassium content of the support precursor. Details of the void formation mechanism will be discussed elsewhere (*32*).

Using the low-dose technique, HREM imaging of the VT-1.9 catalyst showed that the surfaces at an initial stage were clean and without any anomalous surface features (Fig. 8). The same observation was made with the VTM-1.2 sample. The bulk structure seems to extend up to the surface. This observation can be explained by the similar scattering power of the V and Ti atoms and by a similar structure of the support and the deposited vanadium oxide. Alternatively, the vanadium can be present in the support as a solid solution. Determination of the total amount of vanadium and its average oxidation number using titrimetric methods (*15*) showed that the vanadium in VTM-1.2 was present exclusively as V^{4+} species, and in amount corresponding to a complete monolayer. The vanadium oxide of the VT-1.9 catalyst was found to consist of approximately equal amounts of V^{4+} and V^{5+} species. At high vanadium loadings, the amount of V^{4+} always corresponded exactly to a complete monolayer. Since the surface profiles of the VTM-1.2 and VT-1.9 samples did not reveal any difference between the two samples, formation of a solid solution of vanadium in the support seems unlikely because it is well established that vanadium cannot be present as V^{5+} in TiO_2 (*6, 28*). Thus, a reasonable conclusion is that the

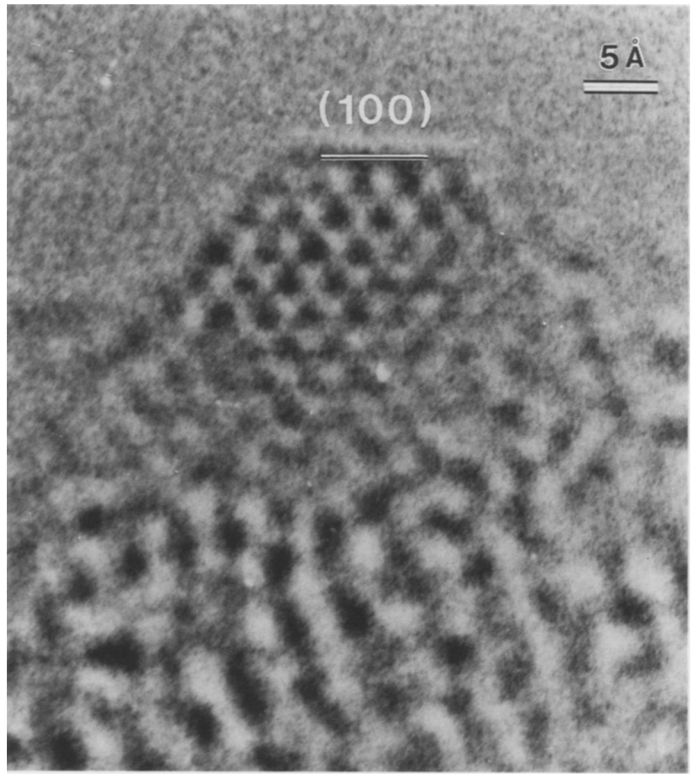

FIG. 9. A particle formed by irradiation of VT-1.9 with the electron beam. Habitus and structure image correspond to a fcc cation lattice. A {100} facet is indicated. Spacings between {111} fringes correspond to VO_x with $x \sim 1$ in ⟨110⟩ projection.

vanadium is present only on top of the support. An oxidation number of V^{4+} for the monolayer suggests that it has a VO_2(B)-like structure, since TiO_2(B) and VO_2(B) are isostructural (*12*). Undoubtedly, the images recorded of TiO_2(B) have structural features that can be recognized in the earlier reported images of VO_2(B) (*18*). The second vana-

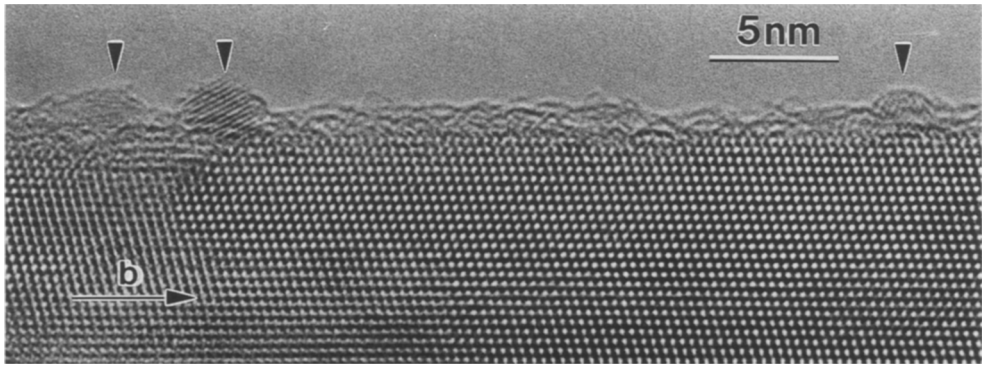

FIG. 10. A surface of the VTM-1.2 sample with particle formation in an initial stage. The direction of the *b*-axis is indicated.

dium layer on top of the monolayer, then, could possibly have a structure related to that of crystalline V_2O_5. It has been demonstrated that a crystallographic fit exists between the (010) faces of V_2O_5 and the (001) faces of TiO_2(B) (*13*). The growth pattern suggested is not, however, directly supported by the features of the IR spectra of the two samples considered.

The spectrum for the VT-1.9 sample has two bands at 835 and 960 cm^{-1}, respectively (Fig. 11). Also, the VT-0.6 and VT-0.9 samples were found to have bands at the same positions (not shown), which are observed typically in the case of compounds having V^{5+} ions in tetrahedral coordination. Vanadinite, $Pb_5(VO_4)_3Cl$, has a weak band at 966 cm^{-1} and a strong band at 833 cm^{-1} (*33*). Also in the case of metavanadates, which are built up from tetrahedral chains (*34*), bands from V=O and V—O—V stretching vibrations are at almost the same wavenumbers (*35*). In the spectrum of the monolayer sample, VTM-1.2, bands are at 820 and 1000 cm^{-1} (Fig. 11). The dominant band at 820 cm^{-1} is shifted 15 cm^{-1} toward lower wavenumbers compared with the strong band at 835 cm^{-1} of the VT-1.9 spectrum. Such a shift, when compared with the band positions of isolated $(VO_4)^{3-}$ and $(VO_4)^{4-}$ species (*36*), indicates that the monolayer is built up from tetrahedrally coordinated V^{4+} species. In comparison with the features revealed in the HREM micrographs, the existence of a few layers of tetrahedrally coordinated vanadium species on top of the support may seem surprising, since the cation in TiO_2(B) and VO_2(B) is in octahedral coordination (*12, 37*) and in V_2O_5 it is in square pyramidal coordination (*14*). Additionally, the infrared spectra shown in Fig. 11 are different from those of VO_2(B) and crystalline V_2O_5 (*18*). However, the surface images, e.g., Figs. 3 and 8, clearly show that the surfaces are not perfectly planar, but irregular. Thus, most likely, many surface cations are strongly under-coordinated compared with those in bulk positions, a fact which can explain the existence of tetrahedrally coordinated surface species. The choice of coordination used to describe cations in metal oxides is to some extent arbitary, and depends upon the ascribed length of the metal–oxygen distances. Therefore, the tetrahedral surface species can possibly be in the neighborhood of four close and two more distant positioned oxygens.

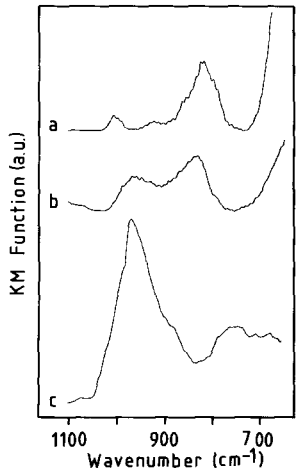

FIG. 11. Diffuse reflectance FTIR difference spectra of the vanadium–oxygen vibration region for (a) VTM-1.2, (b) VT-1.9, and (c) VT-12.4.

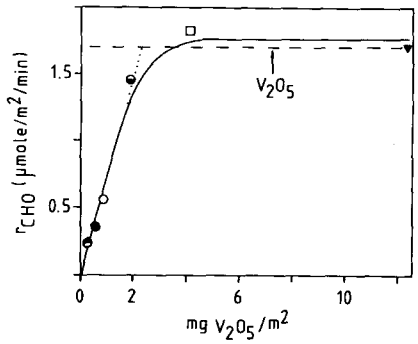

FIG. 12. Rate for formation of benzaldehyde at 370°C versus loading of support. Dashed line: V_2O_5. ⊖ VT-0.3; ● VT-0.6; ○ VT-0.9; ⊖ VT-1.9; □ VT-4.2; and ▼ VT-12.4.

TiO_2(B) surfaces were found to be unstable in a fully converged electron beam, resulting in particle formation (Fig. 4). The particles are probably TiO, which is reason-

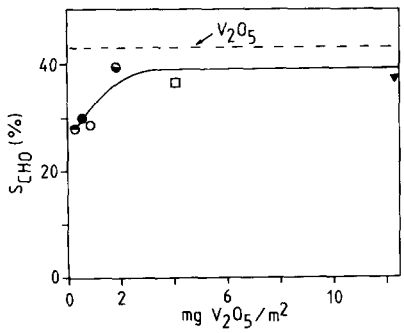

FIG. 13. Selectivity for formation of benzaldehyde at 370°C toward loading of support. Dashed line: V_2O_5. Notations as in Fig. 12.

able considering the observation that beam-induced reduction of TiO_2(rutile) to TiO is possible (*23, 24*). In the present investigation, it was observed that the rate of particle formation was enhanced in the presence of vanadium on the support. The rate was approximately the same for the VTM-1.2 and VT-12.4 samples, while during investigation of some parts of the VT-1.9 sample, it was found to be comparable to the rate observed in the case of the pure support. This fact clearly indicates that the surfaces of the former samples were completely covered with vanadia and that the surface of the latter sample was only partly covered, which is in agreement with the results of our previous investigation (*15*). The vanadia particles, formed as a result of a reduction process, were found to consist of VO_x, with $0.8 \leq x \leq 1.2$ (*25*). Previously, a beam-induced transition of V_2O_5 to $VO_{0.9}$ has been reported (*23, 24*) as well as of TiO_2(anatase)-supported V_2O_5 to an unidentified superstructure (*38*).

The IR spectrum of the catalyst with the highest vanadium loading, VT-12.4, showed the presence of crystalline V_2O_5. After subtraction of the V_2O_5 and support spectra, the difference spectrum obtained indicated the presence of an amorphous phase with short-range order. The broadness of the strong band at 970 cm^{-1} (Fig. 11) implies that it originates from a material having a rather wide distribution of V=O bond lengths. Also, the band at 764 cm^{-1}, which is a V—O—V stretching vibration band (*39*), is very weak, showing the absence of well-defined V—O—V distances. The presence of an amorphous phase together with crystalline V_2O_5 is in agreement with the features discovered in the HREM micrographs. Figure 7 shows the presence of both crystalline and amorphous particles which were not formed as a result of exposure to the electron beam. Chemical analysis of the vanadium, after dissolution in NH_3(aq), showed that the particles had V_2O_5 stoichiometry. In addition to the large particles, a thin vanadium oxide layer must also be present. This conclusion is evidenced by the fact that beam-induced particle formation, similar to the one observed for the VTM-1.2 and VT-1.9 samples, occurred after prolonged exposure to the electron beam of initially apparently homogeneous surfaces (Fig. 6). Unlike earlier reports of V_2O_5 on anatase (*16*), no epitaxy between *in situ* formed vanadium oxide particles and TiO_2(B) support was observed. No homogenous amorphous layer of vanadium oxide covering the support could be detected, unlike the case of anatase as support (*17*).

Catalytic Performance

Considering the activity data in Fig. 12, it is seen that at low vanadium loadings there is an almost linear dependence between the loading and the rate of formation of benzaldehyde. At high loadings, the rate is about the same as that for the V_2O_5 reference sample. If the dependence observed at low loadings is extended as shown by the dotted line in Fig. 12, it is seen that a value equal to that for V_2O_5 is reached at 2.3 mg V_2O_5/m^2, corresponding to approximately 2 theoretical vanadium layers. In our previous investigation (*15*), we found that the coverage of support rapidly increased with increase in loading, with up to 80% coverage at 1.9 mg V_2O_5/m^2. Thus, the low rates obtained at low loadings are due to the support being not completely covered with active phase.

The activity data indicate that full coverage is obtained at a loading corresponding to two theoretical layers. The selectivity dependence in Fig. 13 shows that the selectivity for formation of aldehyde increases from about 30% up to about 39% with increase in vanadium loading. This increase was mainly due to decrease in carbon oxide formation. For the V_2O_5 sample, the selectivity is 43%. The low selectivity at low loadings can be due to degradation of reaction intermediates at exposed titania sites, in agreement with earlier observations (*3, 4*).

As a support for vanadium oxide, it seems that TiO_2(B), when compared with anatase, is less suitable for use in the selective oxidation of toluene to benzaldehyde. Over V_2O_5/TiO_2(anatase) catalysts, the rate and selectivity for aldehyde formation were also found to increase with increase in vanadium content (*5*). At high loadings, the total rate was comparable with the rate for crystalline V_2O_5. However, at best, a selectivity of 67% was reported for aldehyde formation, to be compared with a value of 51% over crystalline V_2O_5 under the same conditions. If the fraction of coverage and support effects are accounted for, the data presented in Figs. 12 and 13 are interesting in that they indicate that the rate and the selectivity for aldehyde formation are independent of the vanadium content. Considering our finding that the structure of the active phase largely depends on the vanadium loading, it seems that the oxidation of toluene to benzaldehyde is structure insensitive. This is, however, not completely true since only carbon oxides were formed over the monolayer catalyst prepared by NH_3(aq)-treatment, VTM-1.2, a result which indicates that the active phase on the VT-0.3, VT-0.6, VT-0.9, and VT-1.9 catalysts preferentially consisits of a few vanadia layers. The results on the oxidation of toluene are different from those obtained in the ammoxidation of the same compound to benzonitrile (*15*). In the latter case, both the activity and the selectivity were strongly structure dependent and an enhancement of the catalytic performance compared with that of pure V_2O_5 was obtained using TiO_2(B) as support.

When heating TiO_2(B)-supported vanadium oxide samples under nitrogen, a temperature dependent transformation of TiO_2(B) to anatase and/or rutile occurred above 525°C (*13*). Under the conditions of (amm)oxidation, however, we have not found any evidence of transformation of TiO_2(B) support when used at 400°C and below for 3 days.

ACKNOWLEDGMENTS

Financial support from the National Swedish Board for Technical Development (STU) and the National Energy Administration (STEV) is gratefully acknowledged.

REFERENCES

1. Bond, G. C., and Brückman, K., *Faraday Discuss. Chem. Soc.* **72,** 235 (1981).
2. Gasior, M., Gasior, I., and Grzybowska, B., *Appl. Catal.* **10,** 87 (1984).
3. Wachs, I. E., Saleh, R. Y., Chan, S. S., and Chersich, C. C., *Appl. Catal.* **15,** 339 (1985).
4. van Hengstum, A. J., van Ommen, J. G., Bosch, H., and Gellings, P. J., *Appl. Catal.* **8,** 369 (1983).
5. Jonson, B., Rebenstorf, B., Larsson, R., and Andersson, S. L. T., *J. Chem. Soc. Faraday Trans. 1* **84,** 3547 (1988).
6. Andersson, A., and Andersson, S. L. T., *in* "Solid State Chemistry in Catalysis" (R. K. Grasselli, and J. F. Brazdil, Eds.), ACS Symposium Series, Vol. 279, p. 121. American Chemical Society, Washington, D.C., 1985.
7. Cavani, F., Foresti, E., Trifirò, F., and Busca, G., *J. Catal.* **106,** 251 (1987).
8. Haber, J., Machej, T., and Czeppe, T., *Surf. Sci.* **151,** 301 (1985).
9. Gasior, M., Haber, J., and Machej, T., *Appl. Catal.* **33,** 1 (1987).
10. Véjux A., and Courtine, P., *J. Solid State Chem.* **23,** 93 (1978).
11. Cavani, F., Centi, G., Parrinello, F., and Trifirò, F., *in* "Preparation of Catalysts IV" (B. Delmon, P. Grange, P. A. Jacobs, and G. Poncelet, Eds.), Studies in Surface Science and Catalysis, Vol. 31, p. 227. Elsevier, Amsterdam, 1987.
12. Marchand, R., Brohan, L., and Tournoux, M. *Mater. Res. Bull.* **15,** 1129 (1980).
13. Papachryssanthou, J., Bordes, E., Véjux, A., Courtine, P., Marchand, R., and Tournoux, M., *Catal. Today* **1,** 219 (1987).
14. Bachmann, H. G., Ahmed, F. R., and Barnes, W. H., *Z. Kristallogr.* **115,** 110 (1961).

15. Sanati, M., and Andersson, A., *J. Mol. Catal.* **59,** 233 (1990).
16. Kang, Z. C., and Bao, Q. X., *Appl. Catal.* **26,** 251 (1986).
17. Baiker, A., Dollenmeier, P., Glinski, M., and Reller, A., *Appl. Catal.* **35,** 351 (1987).
18. Andersson, A., Bovin, J.-O., and Walter, P., *J. Catal.* **98,** 204 (1986).
19. Kirk-Othmer, "Encyclopedia of Chemical Technology," 3rd ed., Vol. 3, p. 740. Wiley, New York, 1978.
20. Powder Diffraction File, JCPDS International Centre for Diffraction Data, Swarthmore, 1985.
21. Andersson, A., and Hansen, S., *J. Catal.* **114,** 332 (1988).
22. Dion, M., Piffard, Y., and Tournoux, M., *J. Inorg. Nucl. Chem.* **40,** 917 (1987).
23. Smith, D. J., McCartney, M. R., and Bursill, L. A., *Ultramicroscopy* **23,** 299 (1987).
24. McCartney, M. R., and Smith, D. J., *Surf. Sci.* **221,** 214 (1989).
25. Andersson, B., Gjonnes, J., and Tafto, J., *Acta Crystallogr. A* **30,** 216 (1974).
26. Matsuda, S., and Kato, A., *Appl. Catal.* **8,** 149 (1983).
27. Busca, G., Saussey, H., Saur, O., Lavalley, J. C., and Lorenzelli, V., *Appl. Catal.* **14,** 245 (1985).
28. Bond, G. C., Sárkány, A. J., and Parfitt, G. D., *J. Catal.* **57,** 476 (1979).
29. Andersson, S. L. T., *J. Chem. Soc. Faraday Trans. 1* **82,** 1537 (1986).
30. Cavani, F., Centi, G., Foresti, E., Trifirò, F., and Busca, G., *J. Chem. Soc. Faraday Trans. 1* **84,** 237 (1988).
31. Wallenberg, L. R., Sanati, M., and Andersson, A., *in* "Electron Microscopy 1990, Proceedings, 12th International Congress for Electron Microscopy, Seattle, 1990," Vol. 4, p. 234. San Francisco Press, San Francisco, 1990.
32. Wallenberg, L. R., Andersson, S., Sanati, M., and Andersson, A., *Microscopy, Microanalysis, Microstructures,* submitted for publication.
33. Griffith, W. P., and Lesniak, P. J. B., *J. Chem. Soc. A* **1066** (1969).
34. Evans, H. T., *Z. Kristallogr.* **114,** 257 (1960).
35. Frederickson, L. D., and Hausen, D. M., *Anal. Chem.* **35,** 818 (1963).
36. Nakamoto, K., "Infrared and Raman Spectra of Inorganic and Coordination Compounds," 4th ed. Wiley, New York, 1986.
37. Théobald, F., Cabala, R., and Bernard, J., *J. Solid State Chem.* **17,** 431 (1976).
38. Véjux, A., and Courtine, P., *J. Solid State Chem.* **63,** 179 (1986).
39. Barraclough, C. G., Lewis, J., and Nyholm, R. S., *J. Chem. Soc.* **3552** (1959).